

# Spinodal and Equilibrium Global Phase Diagram of the $d=3$ Merged Potts-Cubic-Clock Model: First-Order Equilibrium and Second-Order Spinodal Boundaries with Hidden Topologies from Renormalization-Group Theory

Umut Aıkel<sup>1</sup> and A. Nihat Berker<sup>1,2</sup>

<sup>1</sup>*Faculty of Engineering and Natural Sciences, Kadir Has University, Cibali, Istanbul 34083, Turkey*

<sup>2</sup>*Department of Physics, Massachusetts Institute of Technology, Cambridge, Massachusetts 02139, USA*

A model that merges the Potts, cubic, and clock models is studied in spatial dimension  $d=3$  by renormalization-group theory. Effective vacancies are included in the renormalization-group initial conditions. In the global phase diagram, 5 different ordered phases, namely ferromagnetic, antiferromagnetic, ferrimagnetic, antiferromagnetic, axial, and a disordered phase are found, separated by first- and second-order phase boundaries. 8 different phase diagram cross-sections occur. When the effective vacancies are suppressed, the global spinodal phase diagram is found: All disordering phase transitions become second order, the disordered phase recedes, and 17 different phase diagram cross-sections occur, spinodality thus much enriching ordering behavior. In the spinodal phase diagram, the ferrimagnetic and antiferromagnetic phases have reentrance. The employed renormalization group transformation is exact on the  $d = 3$  dimensional hierarchical model and Migdal-Kadanoff approximate on the cubic lattice.

## I. MERGED: POTTS, CUBIC, CLOCK MODELS

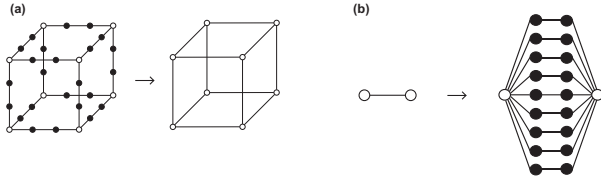


FIG. 1. Exactly solved  $d = 3$  hierarchical lattice and Migdal-Kadanoff: (a) The Migdal-Kadanoff approximate renormalization-group transformation on the cubic lattice. Bonds are removed from the cubic lattice to make the renormalization-group transformation doable. The removed bonds are compensated by adding their effect to the decimated remaining bonds. (b) A hierarchical model is constructed by self-embedding a graph into each of its bonds, *ad infinitum*. [10] The exact renormalization-group solution proceeds in the reverse direction, by summing over the internal spins shown with the dark circles. Here is the most used, so called "diamond" hierarchical lattice [10–13]. The length-rescaling factor  $b$  is the number of bonds in the shortest path between the external spins shown with the open circles,  $b = 3$  in this case. The volume rescaling factor  $b^d$  is the number of bonds replaced by a single bond,  $b^d = 27$  in this case, so that  $d = 3$ .

The mergure of the much used Potts, cubic, clock models is realized by the Hamiltonian

$$\begin{aligned}
 -\beta\mathcal{H} = & \sum_{\langle ij \rangle} -\beta\mathcal{H}_{ij}(\vec{s}_i, \vec{t}_i; \vec{s}_j, \vec{t}_j) = \\
 & \sum_{\langle ij \rangle} \{ J \delta(\vec{s}_i, \vec{s}_j) + K [\delta(\vec{s}_i, \vec{s}_j) - \delta(\vec{s}_i, -\vec{s}_j)] + C \vec{s}_i \cdot \vec{s}_j \}
 \end{aligned} \tag{1}$$

where  $\beta = 1/k_B T$ , at site  $i$  the spin  $\vec{s}_i$  can point in  $q$  different directions  $\theta_i = 2\pi n_i/q$  in the  $xy$  plane, with  $n_i = 0, 1, \dots, q-1$  providing the  $q$  different possible states, the delta function  $\delta(\vec{s}_i, \vec{s}_j) = 1(0)$  for  $\vec{s}_i = \vec{s}_j (\vec{s}_i \neq \vec{s}_j)$ , the last term is a vector product, and the sum is over all interacting pairs of nearest-neighbor spins. We independently vary the Potts interaction strength  $J$ , the cubic interaction  $K$ , and the clock interaction strength  $C$  of this merged Potts-cubic-clock model, to obtain the multistructured, equilibrium and spinodal, global phase diagram. In this study,  $q = 6$  is studied.

## II. METHOD: EXACT 3D HIERARCHICAL AND PHYSICAL MIGDAL KADANOFF, WITH CONDENSATION OF EFFECTIVE VACANCIES

We use the global renormalization-group theory of exactly solvable  $d = 3$  hierarchical model and, equivalently, the physically motivated Migdal-Kadanoff approximation, which have been much discussed and much used. These equivalent procedures consists of decimation and bond moving. The above can be rendered algebraically in the most straightforward way by writing the transfer matrix between two neighboring spins,



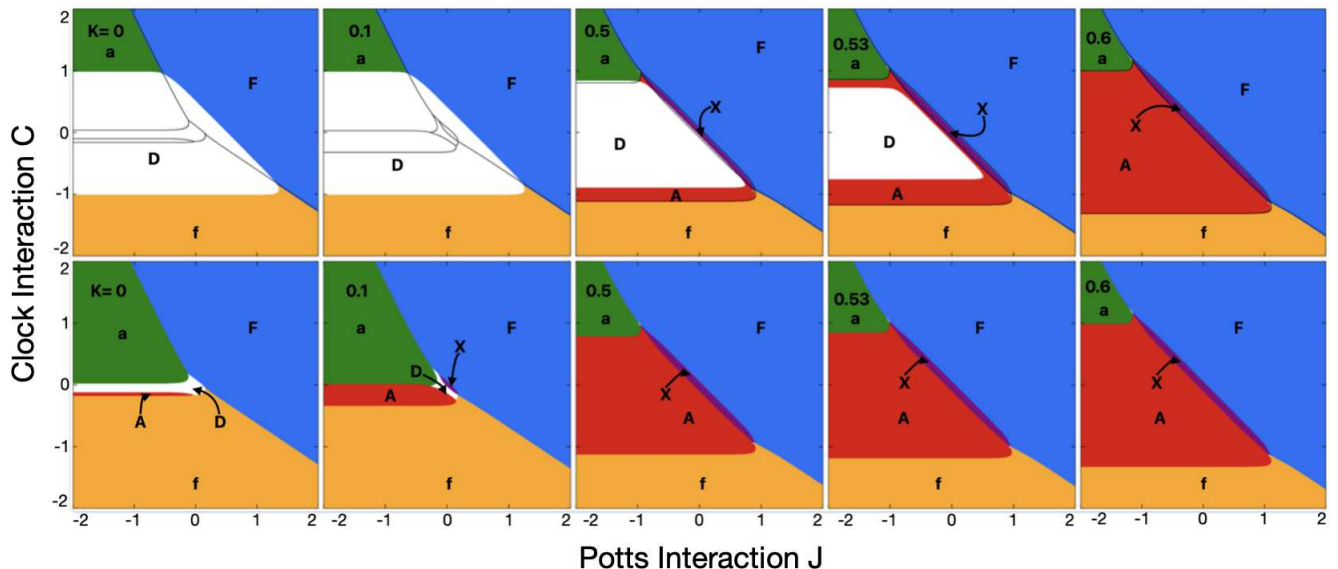


FIG. 3. Calculated spinodal and equilibrium global phase diagram cross-sections, at various fixed values of the cubic interaction  $K$ , of the Potts-cubic-clock model. These constant  $K$  values are given in the upper left of each phase diagram. The ferromagnetic ( $F$ ), antiferromagnetic ( $A$ ), ferrimagnetic ( $f$ ), antiferrimagnetic ( $a$ ), axial ( $X$ ) and disordered ( $D$ ) phases are shown. The top row shows the equilibrium phase diagram. The phase transitions to the disordered phase ( $D$ ) are first order. All other phase boundaries are second order. Three different types of phase diagram topologies, namely the leftmost, middle, rightmost, occur. The lines show the spinodal boundaries. The bottom row shows the spinodal phase diagram, obtained by suppressing the effective vacancies. In the bottom spinodal row, the disordered phase has receded and the disordering transitions are second order, while the other phase transitions remain second order. Three different types of phase diagram topologies occur.

The renormalization-group transformation, explained in Fig. 1, is done with length rescaling factor  $b = 3$  in order to conserve the ferromagnetic-antiferromagnetic symmetry of the method. This method [8, 9] involves decimating three bonds in series into a single bond, followed by bond-moving by superimposing  $b^{d-1} = 9$  bonds. After each algebraic operation, the transfer matrix is divided by its largest element, which amounts to applying a subtractive term to every energy, not affecting the physics but preventing computing overflows. This approach is an approximate solution on the  $d = 3$  cubic lattice and, simultaneously, an exact solution on the  $d = 3$  hierarchical lattice [10–13]. The simultaneous exact solution makes the approximate solution a physically realizable, therefore robust approximation, as also used in turbulence [14], polymer [15], gel [16], electronic system [17] calculations. A physically realizable approximation means that the approximation is exact on an alternate physically realizable system and therefore will obey all the general laws of thermodynamics.

Thus, additional to the exactness on the  $3d$  hierarchical lattice, a simple but effective, physically inspired (see Fig. 1(a)) method in studying phase transitions has been this renormalization-group method under the Migdal-Kadanoff approximation [8, 9]. Thus, using this method on widely different systems, the lower-critical dimension  $d_c$  below which no ordering occurs has been correctly determined as  $d_c = 1$  for the Ising model [8, 9],

$d_c = 2$  for the XY [18, 19] and Heisenberg [20] models, and the presence of an algebraically ordered phase has been seen for the  $d = 2$  XY model [18, 19, 21]. In systems with frozen microscopic disorder (quenched randomness), using the simple Migdal-Kadanoff renormalization-group approximation on quenched random distributions,  $d_c = 2$  has been determined for the random-field Ising [22, 23] and XY models [24], and, yielding a non-integer value,  $d_c = 2.46$  for Ising spin-glass systems [25]. Also under the Migdal-Kadanoff approximation, the chaotic nature of the spin-glass phases [13, 26, 27] has been obtained and quantitatively analyzed, both for quenched randomly mixed ferromagnetic-antiferromagnetic spin glasses [29, 30, 56] and right- and left-chiral (helical) spin glasses [31–33]. The Migdal-Kadanoff procedure has also been used in the calculation of the phase diagrams of surface systems [34], accurately matching experiments with no adjustable parameter, and finite-temperature phase diagrams of high-temperature superconductivity models [35]. For recent works on hierarchical lattices, see Refs.[36–48]

### III. SPINODAL AND EQUILIBRIUM GLOBAL PHASE DIAGRAMS

The phase diagrams are obtained by following the renormalization-group trajectories to their terminus of

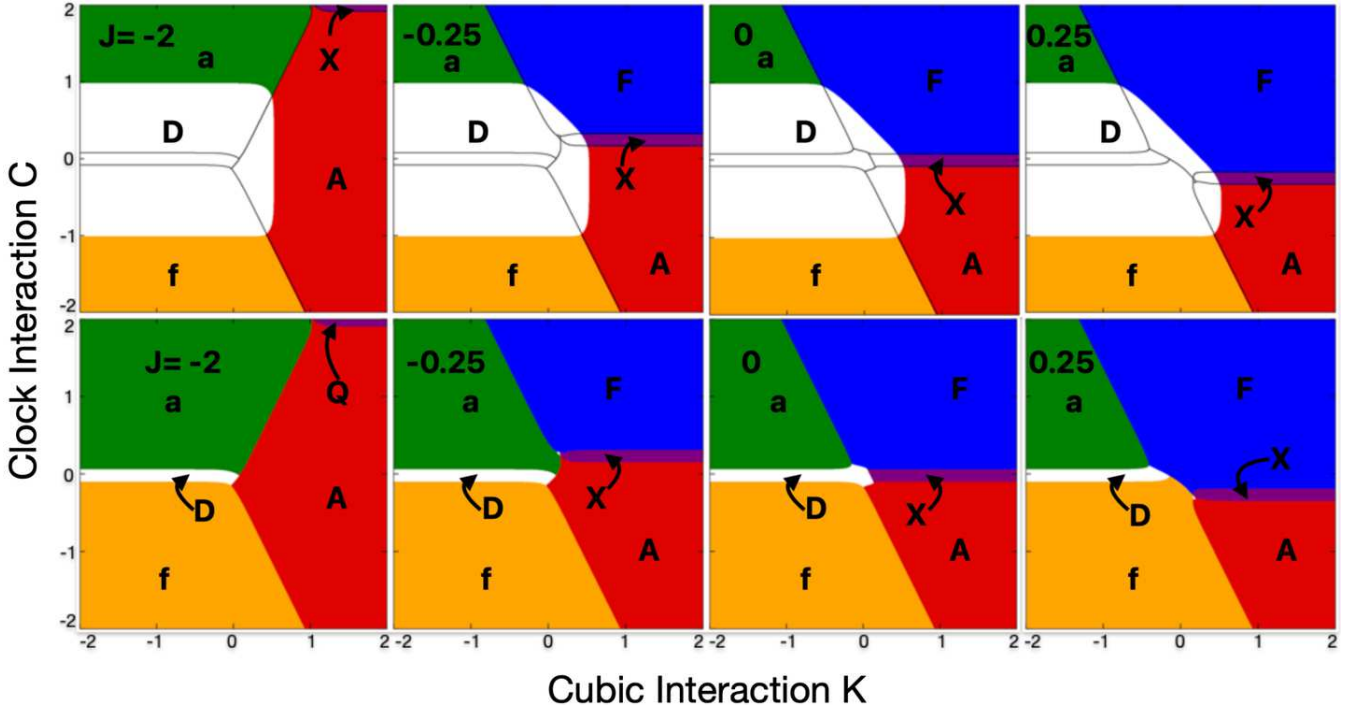


FIG. 4. Calculated spinodal and equilibrium global phase diagram cross-sections, at various fixed values of the Potts interaction  $J$ , of the Potts-cubic-clock model. These constant  $J$  values are given in the upper left of each phase diagram. The ferromagnetic ( $F$ ), antiferromagnetic ( $A$ ), ferrimagnetic ( $f$ ), antiferrimagnetic ( $a$ ), axial ( $X$ ) and disordered ( $D$ ) phases are shown. The top row shows the equilibrium phase diagram. The phase transitions to the disordered phase ( $D$ ) are first order. All other phase boundaries are second order. Two different types of phase diagram topologies, namely the leftmost and rightmost, occur. The lines show the spinodal boundaries. The bottom row shows the spinodal phase diagram, obtained by suppressing the effective vacancies. In the bottom spinodal row, the disordered phase has receded and the disordering transitions are second order, while the other phase transitions remain second order. We note the rich variety of the spinodal phase diagram topologies: Five different types of phase diagram topologies occur.

totally attractive fixed points, namely sinks, shown in Table I.[49]. The basin of attraction of each fixed point is a thermodynamic phase. A sink epitomizes the thermodynamic phase that it attracts. The seven sinks subtending this global phase diagram are given in Table I. The disordered phase has two sinks, dense disordered and dilute disordered, but no phase transition is correctly seen between them, since this system does not contain physical vacancies.[34]

The fixed point attracting the phase boundary between

two thermodynamic phases determines order of the phase transition and, in the case of a second-order phase transition, the critical exponents.[49] Examples are shown in Table II. The fixed point of a first-order phase transition is the superposition of the sinks of the phases that are bounded. From the calculated values in the fixed point of a second-order phase transition, the derivative matrix (*aka*, the recursion matrix) is calculated. For example, for the phase transition between the ferromagnetic and disordered phases in Table II,

$$\begin{pmatrix} \partial A'/\partial A & \partial A'/\partial B & \partial A'/\partial C \\ \partial B'/\partial A & \partial B'/\partial B & \partial B'/\partial C \\ \partial C'/\partial A & \partial C'/\partial B & \partial C'/\partial C \end{pmatrix} = \begin{pmatrix} -0.12001 & -0.50364 & -0.75268 \\ 0.56100 & 1.62461 & 2.12328 \\ 0.28128 & 0.88026 & 1.19962 \end{pmatrix} \quad (4)$$

The eigenvalues of this matrix are  $\lambda_1 = 2.61438$ ,  $\lambda_2 = 0.08618$ ,  $\lambda_3 = 0.00366$ . The latter two eigenvalues are, as expected, less than unity (irrelevant), their right eigenvectors corresponding to renormalization-group flow at-

tractive directions. The leading eigenvalue is greater than unity, relevant, its right eigenvector pointing on either side to the bounded phases. The eigenvalue exponent,

$$y_1 = \ln(\lambda_1)/\ln(b) = 0.874, \quad (5)$$

Renormalization-Group Sinks of the Thermodynamic Phases

$\begin{pmatrix} 1 & 0 & 0 & 0 & 0 & 0 & 0 \\ 0 & 1 & 0 & 0 & 0 & 0 & 0 \\ 0 & 0 & 1 & 0 & 0 & 0 & 0 \\ 0 & 0 & 0 & 1 & 0 & 0 & 0 \\ 0 & 0 & 0 & 0 & 1 & 0 & 0 \\ 0 & 0 & 0 & 0 & 0 & 1 & 0 \\ 0 & 0 & 0 & 0 & 0 & 0 & 1 \end{pmatrix}$	$\begin{pmatrix} 0 & 0 & 0 & 1 & 0 & 0 & 0 \\ 0 & 0 & 0 & 0 & 1 & 0 & 0 \\ 0 & 0 & 0 & 0 & 0 & 1 & 0 \\ 1 & 0 & 0 & 0 & 0 & 0 & 0 \\ 0 & 1 & 0 & 0 & 0 & 0 & 0 \\ 0 & 0 & 1 & 0 & 0 & 0 & 0 \\ 0 & 0 & 0 & 0 & 0 & 0 & 0 \end{pmatrix}$	$\begin{pmatrix} 1 & 0 & 1 & 0 & 1 & 0 & 0 \\ 0 & 1 & 0 & 1 & 0 & 1 & 0 \\ 1 & 0 & 1 & 0 & 1 & 0 & 0 \\ 0 & 1 & 0 & 1 & 0 & 1 & 0 \\ 1 & 0 & 1 & 0 & 1 & 0 & 0 \\ 0 & 1 & 0 & 1 & 0 & 1 & 0 \\ 1 & 0 & 1 & 0 & 1 & 0 & 0 \end{pmatrix}$	$\begin{pmatrix} 0 & 1 & 0 & 1 & 0 & 1 & 0 \\ 1 & 0 & 1 & 0 & 1 & 0 & 0 \\ 0 & 1 & 0 & 1 & 0 & 1 & 0 \\ 1 & 0 & 1 & 0 & 1 & 0 & 0 \\ 0 & 1 & 0 & 1 & 0 & 1 & 0 \\ 1 & 0 & 1 & 0 & 1 & 0 & 0 \\ 0 & 0 & 0 & 0 & 0 & 0 & 0 \end{pmatrix}$
Ferromagnetic (F)	Antiferromagnetic (A)	Ferrimagnetic (f)	Antiferrimagnetic (a)
$\begin{pmatrix} 1 & 0 & 0 & 1 & 0 & 0 & 0 \\ 0 & 1 & 0 & 0 & 1 & 0 & 0 \\ 0 & 0 & 1 & 0 & 0 & 1 & 0 \\ 1 & 0 & 0 & 1 & 0 & 0 & 0 \\ 0 & 1 & 0 & 0 & 1 & 0 & 0 \\ 0 & 0 & 1 & 0 & 0 & 1 & 0 \\ 0 & 0 & 0 & 0 & 0 & 0 & 0 \end{pmatrix}$	$\begin{pmatrix} 1 & 1 & 1 & 1 & 1 & 1 & 0 \\ 1 & 1 & 1 & 1 & 1 & 1 & 0 \\ 1 & 1 & 1 & 1 & 1 & 1 & 0 \\ 1 & 1 & 1 & 1 & 1 & 1 & 0 \\ 1 & 1 & 1 & 1 & 1 & 1 & 0 \\ 1 & 1 & 1 & 1 & 1 & 1 & 0 \\ 0 & 0 & 0 & 0 & 0 & 0 & 0 \end{pmatrix}$	$\begin{pmatrix} 0 & 0 & 0 & 0 & 0 & 0 & 0 \\ 0 & 0 & 0 & 0 & 0 & 0 & 0 \\ 0 & 0 & 0 & 0 & 0 & 0 & 0 \\ 0 & 0 & 0 & 0 & 0 & 0 & 0 \\ 0 & 0 & 0 & 0 & 0 & 0 & 0 \\ 0 & 0 & 0 & 0 & 0 & 0 & 0 \\ 0 & 0 & 0 & 0 & 0 & 0 & 1 \end{pmatrix}$	
Axial (X)	Disordered (D)	Disordered (D)	

TABLE I. Under repeated renormalization-group transformations, the phase diagram points of the phases of the merged Potts-cubic-clock model flow to the sinks shown on this Table giving the exponentiated nearest-neighbor Hamiltonians, namely the transfer matrices. The designations,  $F, A, f, a, X, D$  in Figs. 2-5 are also shown.

Examples Renormalization-Group Fixed Points of Phase Transitions between Thermodynamic Phases

$\begin{pmatrix} 1 & 0 & 0 & 0 & 0 & 0 & 0 \\ 0 & 1 & 0 & 0 & 0 & 0 & 0 \\ 0 & 0 & 1 & 0 & 0 & 0 & 0 \\ 0 & 0 & 0 & 1 & 0 & 0 & 0 \\ 0 & 0 & 0 & 0 & 1 & 0 & 0 \\ 0 & 0 & 0 & 0 & 0 & 1 & 0 \\ 0 & 0 & 0 & 0 & 0 & 0 & 1 \end{pmatrix}$	$\begin{pmatrix} 1 & A & B & C & B & A \\ A & 1 & A & B & C & B \\ B & A & 1 & A & B & C \\ C & B & A & 1 & A & B \\ B & C & B & A & 1 & A \\ A & B & C & B & A & 1 \end{pmatrix}$	$\begin{pmatrix} 1 & 0 & 0 & 0.924 & 0 & 0 \\ 0 & 1 & 0 & 0 & 0.924 & 0 \\ 0 & 0 & 1 & 0 & 0 & 0.924 \\ 0.924 & 0 & 0 & 1 & 0 & 0 \\ 0 & 0.924 & 0 & 0 & 1 & 0 \\ 0 & 0 & 0.924 & 0 & 0 & 1 \end{pmatrix}$
Equilibrium First-Order	Spinodal Second-Order	Equilibrium Second-Order Phase Transition
Ferromagnetic (F) - Disorder (D)	Ferromagnetic (F) - Disorder (D)	Ferromagnetic (F) - Axial (X)

TABLE II. These fixed points attract, under renormalization-group flows, their respective phase boundaries. Under renormalization-group flows, these fixed points have one unstable (namely outflowing) direction, into the two phases they bound, respectively in the opposite flow directions. The calculated values are  $A = 0.96156$ ,  $B = 0.88572$ ,  $C = 0.84832$ .

yields the correlation-length critical exponent,

$$\nu = 1/y_1 = 1.14. \quad (6)$$

Figure 2 shows the calculated spinodal and equilibrium global phase diagram cross-sections, at various fixed values of the clock interaction  $C$ , of the Potts-cubic-clock model. The ferromagnetic ( $F$ ), antiferromagnetic ( $A$ ), ferrimagnetic ( $f$ ), antiferrimagnetic ( $a$ ), axial ( $X$ ), and disordered ( $D$ ) phases are seen. Since a sink epitomizes the thermodynamic phase that it attracts, it is seen that, in the axial phase, the spins preferentially point in  $\pm a$  spin-space directions. Thus this phase is threefold degenerate and its ground state has an entropy of  $\ln 2$  per bond. The ferrimagnetic phase has spins pointing in three spin-space directions separated by  $2\pi/3$ , is therefore doubly degenerate and with ground-state entropy of  $\ln 3$  per bond. The antiferrimagnetic phase forms two such sublattices, is also doubly degenerate and with ground-state

entropy of  $\ln 3$  per bond. The ferromagnetic and antiferromagnetic phases show reentrance [50–58], meaning the disappearance and reappearance of a phase, when proceeding in the phase diagram along a straight line emerging from infinite temperature ( $J = M = 0$ ).

The top row in Fig. 2 shows the equilibrium phase diagram. The phase transitions to the disordered phase ( $D$ ) are first order. All other phase boundaries are second order. Three different types of phase diagram topologies, namely the leftmost, middle, rightmost, occur. The superimposed lines in the top row show the spinodal boundaries. The bottom row shows the spinodal phase diagram, obtained by suppressing the effective vacancies. The disordered phase recedes and the disordering transitions are second order, while the other phase transitions remain second order. Five different types of phase diagram topologies appear.

Figure 3 shows the calculated spinodal and equilibrium



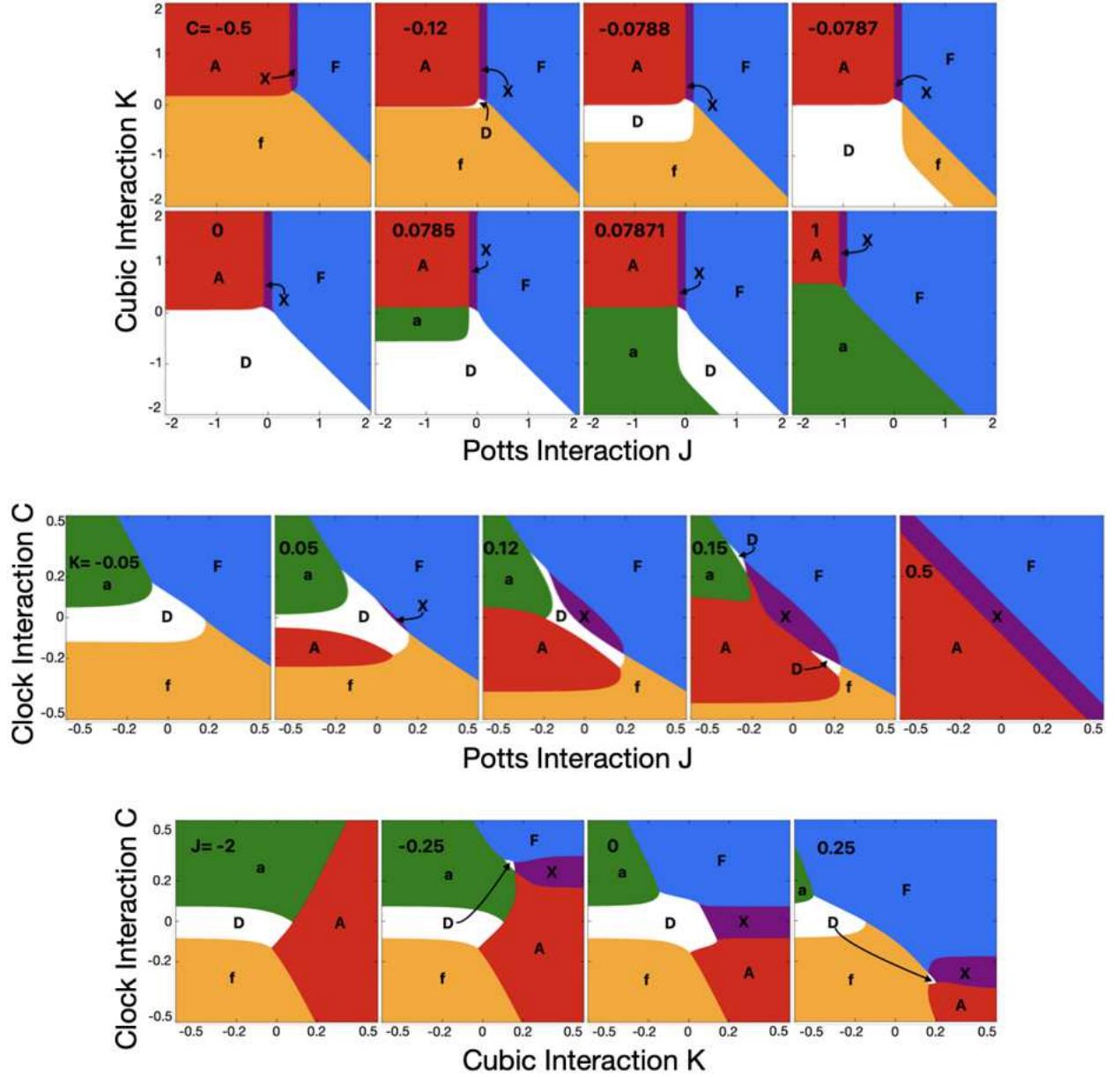


FIG. 5. Topologically distinct cross-sections of the spinodal global phase diagram. The all phase transitions are second order. 17 different phase diagram topologies are seen.

global phase diagram cross-sections, at various fixed values of the cubic interaction  $K$ , of the Potts-cubic-clock model. The top row shows the equilibrium phase diagram. The phase transitions to the disordered phase (D) are first order. All other phase boundaries are second order. Three different types of phase diagram topologies, namely the leftmost, middle, rightmost, occur. The superimposed lines in the top row show the spinodal boundaries. The bottom row shows the spinodal phase diagram, obtained by suppressing the effective vacancies. The disordered phase recedes and the disordering transitions are second order, while the other phase transitions remain second order. Three different types of phase dia-

gram topologies occur.

Figure 4 shows the calculated spinodal and equilibrium global phase diagram cross-sections, at various fixed values of the Potts interaction  $J$ , of the Potts-cubic-clock model. The top row shows the equilibrium phase diagram. The phase transitions to the disordered phase (D) are first order. All other phase boundaries are second order. Two different types of phase diagram topologies, namely the leftmost and rightmost, occur. The superimposed lines in the top row show the spinodal boundaries. The bottom row shows the spinodal phase diagram, obtained by suppressing the effective vacancies. The disordered phase recedes and the disordering transi-

tions are second order, while the other phase transitions remain second order. Four different types of phase diagram topologies occur.

It is thus seen that the spinodal global phase diagram has a much richer phase boundary structure than the equilibrium global phase diagram. The rich phase boundary structure of the spinodal phase diagram gets preempted by the first order transitions under equilibrium. The totality of the spinodal phase diagrams is seen in Fig. 5, exhibiting the phase reentrances [50–58] of the ferrimagnetic and antiferrimagnetic phases.

#### IV. CONCLUSION

We have solved, by renormalization-group theory, the merged Potts-cubic-clock model, obtaining the spinodal and equilibrium global phase diagrams. In the equilib-

rium global phase diagram, 5 different ordered phases and a disordered phase are found, separated by first- and second-order phase boundaries. 8 different phase diagram cross-sections occur. In the spinodal global phase diagram, the disordering phase transitions become second order, the order-to-order phase transitions remain second order, the disordered phase recedes, reentrances of two separate phases appear, 17 different phase diagram cross-sections occur. Suppression of the vacancies has been used to obtain the spinodal phase diagram from renormalization-group theory, yielding the richer phase diagram from under the receding disordered phase.

#### ACKNOWLEDGMENTS

Support by the Academy of Sciences of Turkey (TÜBA) is gratefully acknowledged.

- 
- [1] R. J. Baxter, Potts Model at the Critical Temperature, *J. Phys. C: Solid State Phys.* **6**, L445 (1973).
  - [2] F. Y. Wu, The Potts Model, *Rev. Mod. Phys.* **54**, 235 (1982).
  - [3] A. Bazavova, B. A. Berg, and S. Dubey, Phase Transition Properties of 3D Potts Models, *Nuclear Phys. B* **802**, 421 (2008).
  - [4] B. Nienhuis, A.N. Berker, E.K. Riedel, and M. Schick, First- and Second-Order Phase Transitions in Potts Models: Renormalization-Group Solution, *Phys. Rev. Lett.* **43**, 737 (1979).
  - [5] A. N. Berker and D. Andelman, 1st Order and 2nd Order Phase Transitions in Potts Models - Competing Mechanisms, *J. Applied Phys.* **53**, 7923 (1982).
  - [6] H. Y. Devre and A. N. Berker, First-order to second-order phase transition changeover and latent heats of q-state Potts models in  $d=2,3$  from a simple Migdal-Kadanoff adaptation, *Phys. Rev. E* **105**, 054124 (2022).
  - [7] I. Keçoğlu and A. N. Berker, Global Ashkin-Teller Phase Diagrams in Two and Three dimensions: Multicritical Bifurcation versus Double Tricriticality-Endpoint, *Physica A* **30**, 129248 (2023).
  - [8] A. A. Migdal, Phase transitions in gauge and spin lattice systems, *Zh. Eksp. Teor. Fiz.* **69**, 1457 (1975) [*Sov. Phys. JETP* **42**, 743 (1976)].
  - [9] L. P. Kadanoff, Notes on Migdal's recursion formulas, *Ann. Phys. (N.Y.)* **100**, 359 (1976).
  - [10] A. N. Berker and S. Ostlund, Renormalisation-group calculations of finite systems: Order parameter and specific heat for epitaxial ordering, *J. Phys. C* **12**, 4961 (1979).
  - [11] R. B. Griffiths and M. Kaufman, Spin systems on hierarchical lattices: Introduction and thermodynamic limit, *Phys. Rev. B* **26**, 5022R (1982).
  - [12] M. Kaufman and R. B. Griffiths, Spin systems on hierarchical lattices: 2. Some examples of soluble models, *Phys. Rev. B* **30**, 244 (1984).
  - [13] A. N. Berker and S. R. McKay, Hierarchical Models and Chaotic Spin Glasses, *J. Stat. Phys.* **36**, 787 (1984).
  - [14] R. H. Kraichnan, Dynamics of Nonlinear Stochastic Systems, *J. Math. Phys.* **2**, 124 (1961).
  - [15] P. J. Flory, *Principles of Polymer Chemistry* (Cornell University Press: Ithaca, NY, USA, 1986).
  - [16] M. Kaufman, Entropy Driven Phase Transition in Polymer Gels: Mean Field Theory, *Entropy* **20**, 501 (2018).
  - [17] P. Lloyd and J. Oglesby, Analytic Approximations for Disordered Systems, *J. Phys. C: Solid St. Phys.* **9**, 4383 (1976).
  - [18] J. V. José, L. P. Kadanoff, S. Kirkpatrick, and D. R. Nelson, Renormalization, Vortices, and Symmetry-Breaking Perturbations in 2-Dimensional Planar Model, *Phys. Rev. B* **16**, 1217 (1977).
  - [19] A. N. Berker and D. R. Nelson, Superfluidity and Phase Separation in Helium Films, *Phys. Rev. B* **19**, 2488 (1979).
  - [20] E. Tunca and A. N. Berker, Renormalization-group theory of the Heisenberg model in  $d$  dimensions, *Physica A* **608**, 128300 (2022).
  - [21] O. S. Sariyer, Two-Dimensional Quantum-Spin-1/2 XXZ Magnet in Zero Magnetic Field: Global Thermodynamics from Renormalisation Group Theory, *Philos. Mag.* **99**, 1787 (2019).
  - [22] M. S. Cao and J. Machta, Migdal-Kadanoff Study of the Random-Field Ising Model, *Phys. Rev. B* **48**, 3177 (1993).
  - [23] A. Falicov, A. N. Berker, and S. R. McKay, Renormalization-Group Theory of the Random-Field Ising Model in 3 Dimensions, *Phys. Rev. B* **51**, 8266 (1995).
  - [24] K. Akin and A. N. Berker, Lower-Critical Dimension of the Random-Field XY Model and the Zero-Temperature Critical Line, *arXiv:2203.11153 [cond-mat.stat-mech]* (2022).
  - [25] B. Atalay and A. N. Berker, A Lower Lower-Critical Spin-Glass Dimension from Quenched Mixed-Spatial-Dimensional Spin Glasses, *Phys. Rev. E* **98**, 042125 (2018).
  - [26] S. R. McKay, A. N. Berker, and S. Kirkpatrick, Spin-Glass Behavior in Frustrated Ising Models with Chaotic Renormalization-Group Trajectories, *Phys. Rev. Lett.* **48**, 767 (1982).

- [27] S. R. McKay, A. N. Berker, and S. Kirkpatrick, Amorphously Packed, Frustrated Hierarchical Models: Chaotic Rescaling and Spin-Glass Behavior, *J. Appl. Phys.* **53**, 7974 (1982).
- [28] E. Ilker and A. N. Berker, High q-State Clock Spin Glasses in Three Dimensions and the Lyapunov Exponents of Chaotic Phases and Chaotic Phase Boundaries, *Phys. Rev. E* **87**, 032124 (2013).
- [29] E. Ilker and A. N. Berker, Overfrustrated and Underfrustrated Spin Glasses in  $d=3$  and  $2$ : Evolution of Phase Diagrams and Chaos including Spin-Glass Order in  $d=2$ , *Phys. Rev. E* **89**, 042139 (2014).
- [30] E. Ilker and A. N. Berker, Odd q-State Clock Spin-Glass Models in Three Dimensions, Asymmetric Phase Diagrams, and Multiple Algebraically Ordered Phases, *Phys. Rev. E* **90**, 062112 (2014).
- [31] T. Çağlar and A. N. Berker, Chiral Potts Spin Glass in  $d = 2$  and  $3$  Dimensions, *Phys. Rev. E* **94**, 032121 (2016).
- [32] T. Çağlar and A. N. Berker, Devil's Staircase Continuum in the Chiral Clock Spin Glass with Competing Ferromagnetic-Antiferromagnetic and Left-Right Chiral Interactions, *Phys. Rev. E* **95**, 042125 (2017).
- [33] T. Çağlar and A. N. Berker, Phase Transitions Between Different Spin-Glass Phases and Between Different Chaoses in Quenched Random Chiral Systems, *Phys. Rev. E* **96**, 032103 (2017).
- [34] A. N. Berker, S. Ostlund, and F. A. Putnam, Renormalization-Group Treatment of a Potts Lattice Gas for Krypton Adsorbed onto Graphite, *Phys. Rev. B* **9**, 3650 (1978).
- [35] M. Hinczewski and A. N. Berker, Finite-temperature phase diagram of nonmagnetic impurities in high-temperature superconductors using a  $d=3$  tJ model with quenched disorder, *Phys. Rev. B* **78**, 064507 (2008).
- [36] E. C. Artun, D. Sarman, and A. N. Berker, Nematic Phase of the n-Component Cubic-Spin Spin Glass in  $d=3$ : Liquid-Crystal Phase in a Dirty Magnet, *Physica A* **40**, 129709 (2024).
- [37] Y. E. Pektaş, E. C. Artun, and A. N. Berker, Driven and Non-Driven Surface Chaos in Spin-Glass Sponges, *Chaos, Solitons and Fractals* **17**, 114159 (2023).
- [38] J. Clark and C. Lochridge, Weak-disorder limit for directed polymers on critical hierarchical graphs with vertex disorder, *Stochastic Processes Applications* **158**, 75 (2023).
- [39] M. Kotorowicz and Y. Kozitsky, Phase transitions in the Ising model on a hierarchical random graph based on the triangle, *J. Phys. A* **55**, 405002 (2022).
- [40] P. P. Zhang, Z. Y. Gao, Y. L. Xu, C. Y. Wang, and X. M. Kong, Phase diagrams, quantum correlations and critical phenomena of antiferromagnetic Heisenberg model on diamond-type hierarchical lattices, *Quantum Science Technology* **7**, 025024 (2022).
- [41] K. Jiang, J. Qiao, and Y. Lan, Chaotic Renormalization Flow in the Potts model induced by long-range competition, *Phys. Rev. E* **103**, 062117 (2021).
- [42] G. Mograby, M. Derevyagin, G. V. Dunne, and A. Teplyaev, Spectra of perfect state transfer Hamiltonians on fractal-like graphs, *J. Phys. A* **54**, 125301 (2021).
- [43] I. Chio, R. K. W. Roeder, Chromatic zeros on hierarchical lattices and equidistribution on parameter space, *Annales de l'Institut Henri Poincaré D*, **8**, 491 (2021).
- [44] B. Steinhurst and A. Teplyaev, Spectral analysis on Barlow and Evans' projective limit fractals, *J. Spectr. Theory* **11**, 91 (2021).
- [45] A. V. Myshlyavtsev, M. D. Myshlyavtseva, and S. S. Akiemenko, Classical lattice models with single-node interactions on hierarchical lattices: The two-layer Ising model, *Physica A* **558**, 124919 (2020).
- [46] M. Derevyagin, G. V. Dunne, G. Mograby, and A. Teplyaev, Perfect quantum state transfer on diamond fractal graphs, *Quantum Information Processing*, **19**, 328 (2020).
- [47] S.-C. Chang, R. K. W. Roeder, and R. Shrock, q-Plane zeros of the Potts partition function on diamond hierarchical graphs, *J. Math. Phys.* **61**, 073301 (2020).
- [48] C. Monthus, Real-space renormalization for disordered systems at the level of large deviations, *J. Stat. Mech. - Theory and Experiment*, 013301 (2020).
- [49] A. N. Berker and M. Wortis, Blume-Emery-Griffiths-Potts Model in Two Dimensions: Phase Diagram and Critical Properties from a Position-Space Renormalization Group, *Phys. Rev. B* **14**, 4946 (1976).
- [50] P. E. Cladis, New liquid-crystal phase diagram, *Phys. Rev. Lett.* **35**, 48 (1975).
- [51] R. R. Netz and A. N. Berker, Smectic C order, in-plane domains, and nematic reentrance in a microscopic model of liquid crystals, *Phys. Rev. Lett.* **68**, 333 (1992).
- [52] J. O. Indekeu, A. N. Berker, C. Chiang, and C. W. Garland, Reentrant transition enthalpies of liquid crystals: The frustrated spin-gas model and experiments, *Phys. Rev. A* **35**, 1371 (1987).
- [53] C. A. Vause and J. S. Walker, Effects of orientational degrees of freedom in closed-loop solubility phase diagrams, *Phys. Lett. A* **90**, 419 (1982).
- [54] R. G. Caflisch, A. N. Berker, and M. Kardar, Reentrant melting of krypton adsorbed on graphite and the helical Potts-lattice-gas model, *Phys. Rev. B* **31**, 4527 (1985).
- [55] E. F. Sarmento and T. Kaneyoshi, Phase transition of transverse Ising model in a random field, *Phys. Rev. B* **39**, 9555 (1989).
- [56] E. Ilker and A. N. Berker, High q-state clock spin glasses in three dimensions and the Lyapunov exponents of chaotic phases and chaotic phase boundaries, *Phys. Rev. E* **87**, 032124 (2013).
- [57] A. M. Frassino, D. Kubiznak, R. B. Mann, and F. Simovic, Multiple reentrant phase transitions and triple points in Lovelock thermodynamics, *J. High Energy Phys.* **09**, 080 (2014).
- [58] A. Dehghani, S. H. Hendi, and R. B. Mann, Range of novel black hole phase transitions via massive gravity: Triple points and N-fold reentrant phase transitions, *Phys. Rev. D* **101**, 084026 (2020).